mater.scichina.com link.springer.com Published online 30 October 2020 | https://doi.org/10.1007/s40843-020-1499-8
Sci China Mater 2021, 64(4): 798–807

Tailoring organic bulk-heterojunction for charge extraction and spectral absorption in $CsPbBr_3$ perovskite solar cells

Jian Du[1], Jialong Duan[1*], Yanyan Duan[2] and Qunwei Tang[1*]

ABSTRACT **All-inorganic $CsPbBr_3$ perovskite solar cells (PSCs) are promising candidates to balance the stability and efficiency issues of organic-inorganic hybrid devices. However, the large energy barrier for charge transfer and narrow spectral response are still two challenging problems for performance improvement. We present here an organic bulk-heterojunction {poly(3-hexylthiophene-2,5-diyl):[6,6]-phenyl C61 butyric acid methyl ester (P3HT : PCBM)} photoactive layer to boost the charge extraction and to widen the spectral absorption, achieving an enhanced power conversion efficiency up to 8.94% by optimizing the thickness of P3HT: PCBM photoactive layer, which is much higher than 6.28% for the pristine $CsPbBr_3$ device. The interaction between the carbonyl group in PCBM and unsaturated Pb atom in the perovskite surface can effectively passivate the defects and reduce charge recombination. Furthermore, the coupling effect between PCBM and P3HT widens the spectral response from 540 to 650 nm for an increased short-circuit current density. More importantly, the devices are relatively stable over 75 days upon persistent attack by 70% relative humidity in air condition. These advantages of high efficiency, excellent long-term stability, cost-effectiveness and scalability may promote the commercialization of inorganic PSCs.**

Keywords: inorganic $CsPbBr_3$ perovskite solar cells, bulk-heterojunction, charge extraction, spectral absorption, stability

INTRODUCTION

High power conversion efficiency (PCE) and good long-term stability are two persistent objectives to forward photovoltaic commercialization [1,2]. Organic-inorganic hybrid perovskite solar cells (PSCs) have been a new star in the photovoltaic community in recent years. However, the biggest challenge is to overcome the performance degradation under persistent light, heat and/or moisture attack although the certified efficiency of organic-inorganic hybrid PSC is up to 25.2% [3–6]. The complete substitution of organic species such as $CH_3NH_3^+$ (MA^+) or $HC(NH_2)_2^+$ (FA^+) in hybrid perovskites with inorganic Cs^+ to form all-inorganic perovskites demonstrates a great potential to increase the environmental tolerance [7–9]. Among them, all-inorganic $CsPbBr_3$ perovskite with high carrier mobility and stable crystal structure in high-humidity and high-temperature atmospheres is preferred to balance the efficiency and stability for PSC application [10]. Since the birth of the first $CsPbBr_3$ PSC prototype free of hole-transporting layer by replacing precious metal electrodes with a cost-effective carbon electrode in 2016 [10,11], the state-of-the-art all-inorganic $CsPbBr_3$ PSCs have achieved the best PCE (>10%) by optimizing the interfacial charge transfer and perovskite film quality [12–14]. However, the PCEs of these $CsPbBr_3$ solar cells are still much lower than those of state-of-the-art organic-inorganic hybrid PSCs [15], therefore, how to increase the photovoltaic performances of $CsPbBr_3$-based devices is urgent to promote their applications in semitransparent and tandem solar cells.

Generally, the lower PCE of all-inorganic $CsPbBr_3$ PSC is mainly dominated by two reasons [16,17]: (i) the large energy barrier of 0.6 eV at $CsPbBr_3$/carbon interface leads to serious charge carrier recombination; (ii) the wide bandgap of $CsPbBr_3$ halide (2.3 eV) results in a narrow light absorption at wavelength below 540 nm. The use of p-type materials such as poly(3-hexylthiophene-2,5-diyl) (P3HT) and quantum dots is a promising solution to

[1] Institute of New Energy Technology, College of Information Science and Technology, Jinan University, Guangzhou 510632, China
[2] State Centre for International Cooperation on Designer Low-Carbon and Environmental Material (SCICDLCEM), School of Materials Science and Engineering, Zhengzhou University, Zhengzhou 450001, China
[*] Corresponding authors (emails: duanjialong@jnu.edu.cn (Duan J); tangqunwei@jnu.edu.cn (Tang Q))

boost charge extraction [18–20]; however, the narrow light absorption of $CsPbBr_3$ perovskite film is still unchanged. To the best of our knowledge, the fabrication of tandem structure with two or more spectra-complementary sub-cells can undoubtedly solve the aforementioned problems [21,22], but the rigorous requirements on matched currents generated from sub-cells and transparent recombination layer lead to complicated fabrication processes. In order to simplify this scenario, the emerging perovskite/organic bulk-heterojunction (BHJ) solar cells free of recombination layers have attracted considerable interests because of their broad spectral response and high open-circuit voltage (V_{oc}) [23–27]. In this kind of device, two stacked photovoltaic layers including a perovskite bottom layer and an organic BHJ layer are fabricated using orthogonal solvents, in which the BHJ layer composed of an electron donor and acceptor has been widely applied in organic solar cells because of the narrow bandgap and good solubility [28,29]. Liu *et al.* [23] has summarized the recent progresses of the perovskite/BHJ solar cells, demonstrating the feasibility to enhance photovoltaic performance. A significantly enhanced efficiency of 19.0% has been reported so far for the $MAPbI_3$-based PSC [27]. Generally, the performances of organic photovoltaics can be maximized by optimizing molecular structures of donors or acceptors to realize complementary absorption [30]. Following this line of thought, Wu *et al.* [31] has recently increased the PCE from 16.67% to 21.55% by integrating a novel BHJ layer into PSC device, extending the photoresponse of the device to 950 nm. This physical proof-of-concept perovskite/BHJ device is given a mission to minimize the spectral loss and to realize high-performance photovoltaic cell without sacrificing the long-term stability. Therefore, the integration of wide-spectral BHJ layer with stable $CsPbBr_3$ perovskite is a good solution to increase the spectral response of inorganic $CsPbBr_3$ solar cells.

In this work, we have fabricated an organic P3HT:[6,6]-phenyl C61 butyric acid methyl ester (PCBM) BHJ layer and assembled it into inorganic $CsPbBr_3$ PSC by a spin-coating technique to optimize the perovskite/carbon interface. By regulating the thickness of BHJ layer, the solar cell with an architecture of fluorine-doped tin oxide (FTO)/c-TiO_2/m-TiO_2/$CsPbBr_3$/BHJ/carbon achieves an enhanced PCE as high as 8.94%, which is much higher than 6.28% for the reference device. The performance enhancement is mainly attributed to the boosted charge extraction and broadened light absorption from 540 to 650 nm. More importantly, the solar cell presents improved stability over 75 d without encapsulation under persistent attack by 70% humidity, demonstrating a great superiority to obtain high-performance and stable PSC platforms.

EXPERIMENTAL SECTION

Materials and reagents

Unless stated otherwise, materials and reagents such as $PbBr_2$ (Aladdin; > 99.0%), CsBr (Aladdin; > 99.9%), PCBM (AR; > 99%) and P3HT (AR; 99%) were purchased from Aladdin and used without further purification. FTO glass substrates were obtained from Yinkou Opvtech Co., Ltd. Carbon paste was purchased from Shanghai MaterWin New Materials Co., Ltd.

Preparation of TiO_2 photoanode

FTO glass was etched by zinc powders and HCl for a slender strip pattern, and rinsed with ethanol and deionized water. A layer of c-TiO_2 was deposited on the FTO glass by spin-coating an ethanol solution of titanium isopropoxide (0.5 mol L^{-1}) and diethanol amine (0.5 mol L^{-1}) at 7000 rpm for 30 s. Subsequently, the film was annealed in air at 500°C for 2 h. The m-TiO_2 layer was then deposited by spin-coating a colloidal TiO_2 at 2000 rpm for 30 s and annealed in air at 450°C for 30 min. Then the substrate was immersed into an aqueous solution of 0.04 mol L^{-1} $TiCl_4$ at 70°C for 30 min, rinsed with deionized water and ethanol, and finally annealed at 450°C in air for another 30 min.

Assembly of solar cells

The inorganic $CsPbBr_3$ perovskite film was prepared by a multi-step spin-coating method developed by our group [32]. In detail, *N,N*-dimethylformamide (DMF) solution of 1.0 mol L^{-1} $PbBr_2$ was spin-coated onto the pre-heated m-TiO_2 layer at 2000 rpm for 30 s, followed by drying at 80°C for 30 min. Then, 90 μL of CsBr (0.07 mol L^{-1}) methanol solution was spin-coated onto FTO/c-TiO_2/m-TiO_2/$PbBr_2$ at 2000 rpm for 30 s, and heated at 250°C on a hotplate for 5 min. This step was repeatedly performed for several times until a high-purity $CsPbBr_3$ layer was formed.

The solution of P3HT:PCBM (molar ratio of 1:1) in chlorobenzene was spin-coated on the surface of $CsPbBr_3$ film at 2000 rpm for 30 s, followed by drying at 100°C for 5 min to fabricate a compact BHJ layer. Finally, a carbon back-electrode with an active area of 0.09 cm^2 was covered onto FTO/c-TiO_2/m-TiO_2/$CsPbBr_3$/BHJ layer by a doctor-blade coating method and heated at 70°C for

10 min.

Characterizations and tests

The photocurrent density-voltage (J-V) curves of solar cells were recorded using a solar simulator (Newport, Oriel Class A, 91195A) under AM 1.5G simulated solar illumination (100 mW cm^{-2}, calibrated by a standard silicon solar cell). Ultraviolet-visible (UV-Vis) absorption spectra were obtained with a MATASH ultraviolet-visible spectrometer. The surface morphologies of the prepared films were characterized by a field-emission scanning electron microscope (FESEM, Japan Hitachi field emission S4800). The steady-state photoluminescence (PL) spectra were obtained at room temperature by an FLS920 all-functional fluorescence spectrometer. The incident photon-to-current efficiency (IPCE) spectra of various devices were recorded by IPCE kit developed by Enli Technology Co., Ltd. in the 300–800 nm range at room temperature. The time-resolved PL (TRPL) measurement was carried out using a time-resolved fluorescence spectrometer (Horiba Jobin Yvon, FL).

RESULTS AND DISCUSSION

The inorganic $CsPbBr_3$ solar cell presents a configuration of FTO/c-TiO_2/m-TiO_2/$CsPbBr_3$/carbon free of hole transporting layer, in which the large energy barrier at the $CsPbBr_3$/carbon interface and the large bandgap of 2.3 eV of $CsPbBr_3$ halide are regarded as the crucial origins for sluggish solar-to-electric conversion efficiency [32,33]. By blending P3HT and PCBM to form a BHJ layer, the integrated solar cell with FTO/c-TiO_2/m-TiO_2/$CsPbBr_3$/BHJ/carbon has been successfully fabricated by the solution-processable technology in this work, as shown in Fig. 1a, b. From the cross-sectional SEM image of the typically integrated perovskite/BHJ solar cell, a multilayer structure with the thicknesses of ~560 and ~320 nm for FTO and c-TiO_2/m-TiO_2 layers can be observed, respectively. Notably, the $CsPbBr_3$ layer with a thickness of ~440 nm displays vertical monolayer-aligned grains (~1 μm in horizontal direction as shown in Fig. 1c). This extraordinary morphology contributes to the facile charge transport and reduced energy loss for maximal power output [34]. After spin-coating the BHJ layer, it can be obviously observed that the perovskite is fully covered (Fig. 1c), and the well-defined multilayer structure free of pinholes is beneficial for light absorption along with maximized charge extraction.

To better understand the mechanism of charge transfer within the integrated solar cell, Fig. 1d illustrates the charge transfer processes of P3HT:PCBM BHJ-tailored solar cell [23–27,35], and the energy level distributions are also provided in Fig. 1e. Under solar irradiation, the $CsPbBr_3$ layer absorbs the light with wavelength (λ) < 540 nm and generates electron-hole pairs. Arising from the energy level alignment, the photo-induced electrons in perovskite film flow to the conduction band of TiO_2

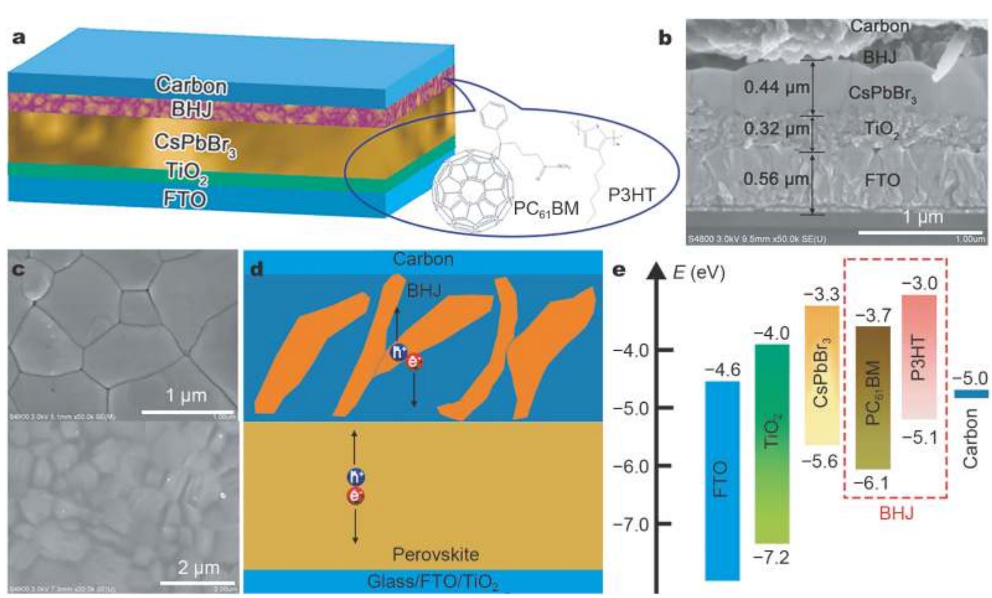

Figure 1 (a) Schematic diagrams of device structure and molecular structure. (b) Cross-sectional SEM image of the integrated perovskite/BHJ device. (c) Top-view SEM images of $CsPbBr_3$ (upper) and $CsPbBr_3$/BHJ (bottom) films. (d) Schematic diagram of charge transfer and (e) the energy level alignment of FTO/c-TiO_2/m-TiO_2/$CsPbBr_3$/BHJ/carbon solar cell.

and then transfer along the percolating TiO_2 pathways under a local electric field, leaving holes to be collected by the donor P3HT in the BHJ layer. The permeated light from the $CsPbBr_3$ film with λ > 540 nm will be re-absorbed by the BHJ layer, realizing the electron-hole separation at the P3HT/PCBM interface. There is a fact that the perovskites possess ambipolar charge transport properties with high hole- and electron-mobilities as well as low recombination loss in the film [36,37]. In this fashion, the electrons generated in the BHJ film can transport along the acceptor molecule (PCBM)-based network to the $CsPbBr_3$ film, and then transfer through the perovskite film to be collected by the cathode, while the holes are collected by the carbon electrode. Due to the large light absorption coefficient of organic BHJ layer, the monolithic device can realize the enhanced power output by integrating bottom perovskite and top BHJ layer into a solar cell.

Fig. 2a displays the characteristic *J*-*V* curves of inorganic $CsPbBr_3$ PSCs measured under one standard sun irradiation (AM1.5, 100 mW cm^{-2}), and the corresponding photovoltaic data are summarized in Table 1. Obviously, the pristine $CsPbBr_3$ PSC only achieves a PCE of 6.28% with a V_{oc} of 1.33 V, short-circuit current density (J_{sc}) of 6.25 mA cm^{-2}, and fill factor (FF) of 75.5%. Upon introducing P3HT as the hole transporting material, the PCE, J_{sc}, V_{oc} and FF are observably enhanced to 7.57%, 1.40 V, 7.11 mA cm^{-2} and 76.1%, respectively. According to previous report [38], the individual P3HT will not contribute to the photocurrent although it has visible absorption. Therefore, the mechanism behind this enhancement is mainly attributed to the accelerated charge extraction owing to the inserted intermediate energy level between the perovskite and carbon electrode [18,39]. By blending P3HT with PCBM to form a donor/acceptor BHJ layer, the device achieves the best PCE up to 8.94% (V_{oc} = 1.50 V, J_{sc} = 7.82 mA cm^{-2}, FF = 76.2%) at an optimal thickness of 110 nm for the BHJ layer. Additionally, the steady power output for characterizing the reliability of *J*-*V* measurements is shown in Fig. S1. A steady-state current density of 7.10 mA cm^{-2} and an efficiency of 8.74% are obtained for the optimized device. The little PCE deviation between steady-state and dynamic-state characterizations is mainly attributed to the existence of hysteresis effect in the device (Fig. S1). The IPCE characterization was further performed to study the

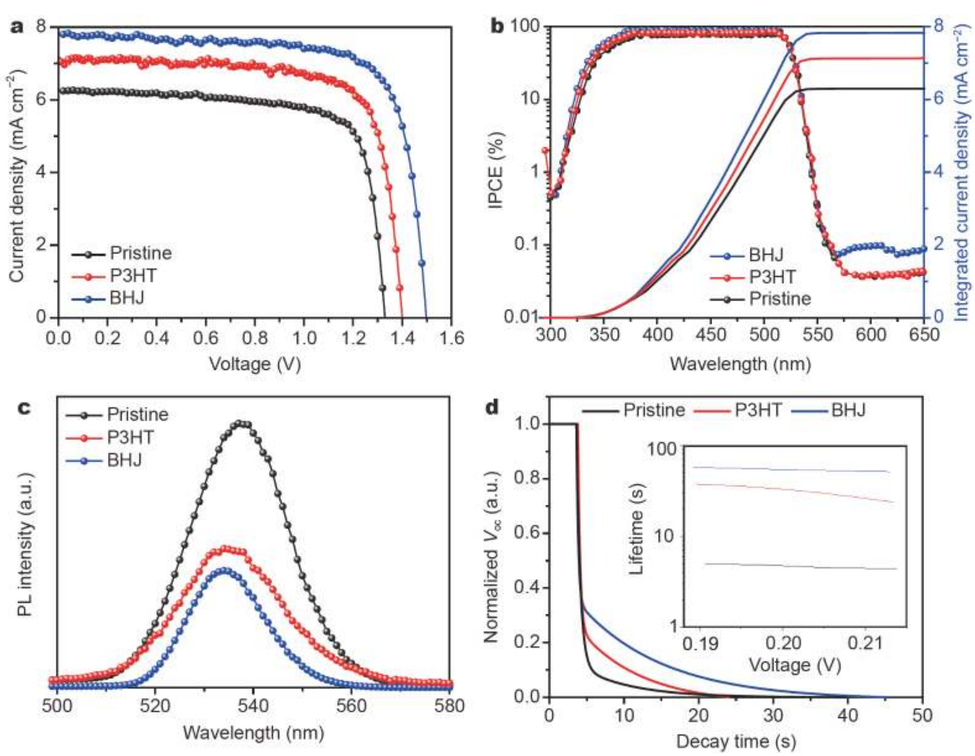

Figure 2 (a) *J*-*V* curves of different devices under one sun illumination. (b) IPCE spectra of different devices. (c) Steady-state PL spectra of FTO/c-TiO_2/m-TiO_2/$CsPbBr_3$, FTO/c-TiO_2/m-TiO_2/$CsPbBr_3$/P3HT and FTO/c-TiO_2/m-TiO_2/$CsPbBr_3$/BHJ films. (d) V_{oc} decay curves and electron lifetimes of different devices.

Table 1 The photovoltaic parameters of various devices under one sun illumination

Devices	Thickness (nm)	V_{oc} (V)	J_{sc} (mA cm^{-2})	FF (%)	PCE (%)
Pristine	–	1.33	6.25	75.5	6.28
P3HT	–	1.40	7.11	76.1	7.57
BHJ	90	1.42	6.33	75.5	6.78
BHJ	100	1.42	6.82	75.6	7.33
BHJ	110	1.50	7.82	76.2	8.94
BHJ	120	1.49	7.31	74.7	8.14

potential mechanism behind the performance enhancement, as shown in Fig. 2b and Fig. S2. In comparison with state-of-the-art organic-inorganic hybrid PSCs, the pristine $CsPbBr_3$ solar cell exhibits a narrow light absorption due to the large bandgap of 2.3 eV. In a wavelength region of 300–540 nm, the maximal IPCE value is ~77% for pristine inorganic PSC and it increases to 80% and 89% for P3HT- and BHJ-based devices, respectively. Notably, the device using $CsPbBr_3$/BHJ as hybrid light harvester shows a photo-response up to 650 nm, which is accordance with the absorption spectra shown in Fig. S3. This enhanced IPCE value cross-checks the efficient electron-hole separation for higher J_{sc} and V_{oc} outputs owing to the accelerated charge extraction and extended light absorption region. The successful realization of physical proof-of-concept photoactive layer provides an opportunity for wide-spectral $CsPbBr_3$ PSCs.

Steady-state PL spectra of the perovskite films with and without organic interlayer were measured to further explore the charge extraction behavior. As shown in Fig. 2c, the FTO/c-TiO_2/m-TiO_2/$CsPbBr_3$/P3HT film demonstrates significant PL quenching at 537 nm in comparison with that of FTO/c-TiO_2/m-TiO_2/$CsPbBr_3$ film, which can be associated with the efficient hole extraction ability of P3HT from the perovskite [40,41]. The highest PL quenching is observed upon introducing the PCBM into the BHJ layer because partial electrons transfer to PCBM from perovskite for a reduced charge radiative recombination. Fig. S4 presents the TRPL plots and the corresponding carrier decay lifetimes (Table S1) are calculated by the double-exponential decay function: $I = Ae^{-(t-t_0)/\tau_1} + Be^{-(t-t_0)/\tau_2}$, where I is the PL intensity at time t, A and B are constants, τ_1 is the faster component of the pure dephasing time of nonradiative recombination, such as the phonon scattering and Auger recombination loss, and τ_2 is the slower component of the exciton spontaneous radiative recombination time [42]. The lifetime is 3.55 ns for FTO/c-TiO_2/m-TiO_2/$CsPbBr_3$ and increases to 4.34 and 4.59 ns for TiO_2/m-TiO_2/$CsPbBr_3$/P3HT and FTO/c-TiO_2/m-TiO_2/$CsPbBr_3$/BHJ, respectively. The longer PL lifetime means suppressed charge nonradiative recombination by setting BHJ layer and indicates the small molecules or polymers in the BHJ film can effectively reduce the defect, which can be also cross-checked by the blue-shift of the PL peak [43,44]. The mechanism behind this phenomenon is mainly attributed to the strong interaction between –C=O group in PCBM and the unsaturated Pb atom in the perovskite, which will be discussed in the following part.

Open-circuit photovoltage decay (OCVD) characterization in Fig. 2d provides deep insights into the recombination process. Briefly, the electron lifetimes (τ_n) are obtained according to the following equations: $\tau_n = kT/q\ (dV_{oc}/dt)^{-1}$, where k is Boltzmann constant, T is absolute temperature, and q is elementary charge [45]. It can be seen that the photovoltage undergoes a rapid decay when switching light off, and the $CsPbBr_3$/BHJ-tailored device decays much slower than the pristine and P3HT-based devices. The longer electron lifetime (inset of Fig. 2d) refers to an inhibited charge recombination and higher charge collection efficiency, which is consistent with the conclusion from PL and TRPL characterizations.

The film thickness has a significant impact on the photovoltaic performance of multilayer-structured solar cell in either light harvest or charge transportation. Fig. 3a compares the characteristic J-V curves of the integrated solar cells with different BHJ thicknesses and the photovoltaic parameters are listed in Table 1. By tuning BHJ thickness from 90 to 120 nm through varying the concentration of BHJ precursor (Table S2), there is a maximal situation at 110 nm with a champion PCE of 8.94% along with excellent reproducibility (Fig. 3b), which may be attributed to the increased carrier mobility and decreased recombination center. In order to quantitatively compare the trap density of solar cell, the hole-only device was fabricated and the dark current was recorded, as shown in Fig. 3c. According to $V_{TFL} = qn_tL^2/2\varepsilon\varepsilon_0$, where trap-filled limit voltage (V_{TFL}) is the voltage kink point, n_t is the trap density, L is the perovskite thickness, ε is the relative dielectric constant of $CsPbBr_3$, and ε_0 is the vacuum permittivity. The smaller V_{TFL} value indicates the lower trap state density [46]. As shown in Fig. 3d, the device with the 110-nm-thickness BHJ layer presents the smallest V_{TFL} value, illustrating that the trap state in perovskite is effectively passivated by the organic BHJ layer. Hall-effect measurement was also conducted and presented in Fig. 3d. The carrier mobility is highly dependent on the thickness of BHJ layer and it presents the

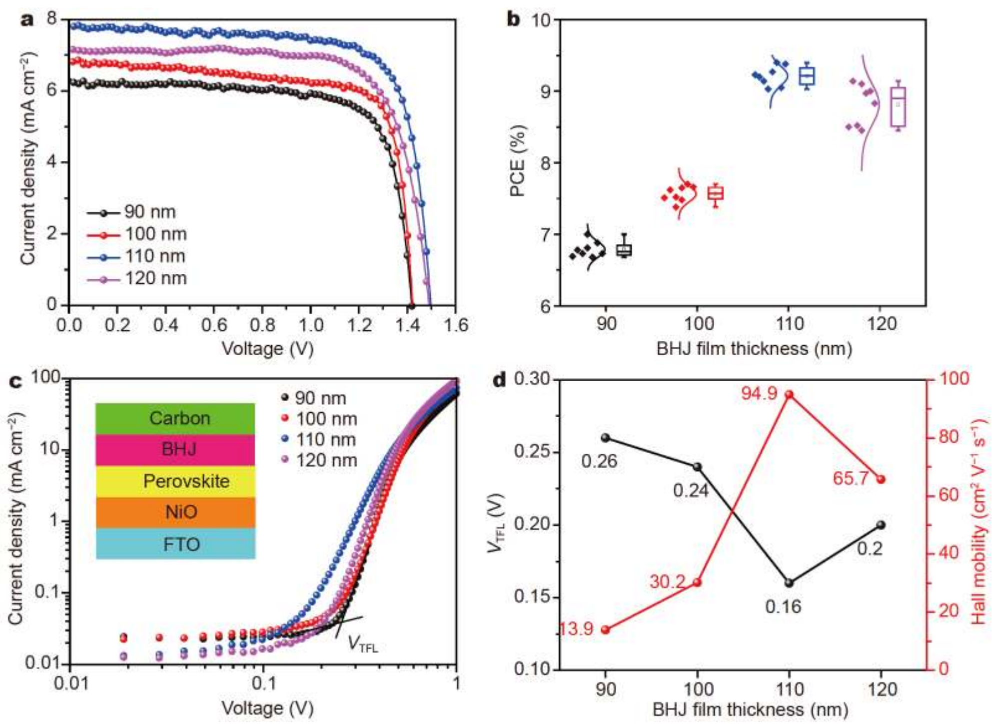

Figure 3 (a) *J-V* curves of FTO/c-TiO_2/m-TiO_2/$CsPbBr_3$/BHJ/carbon devices with different BHJ thicknesses. (b) PCE distributions of the BHJ-tailored solar cells at different thicknesses. (c) Dark current-voltage curves from hole-only devices in the inset. (d) The V_{TFL} and Hall mobility *versus* BHJ thickness.

highest value up to 94.9 $cm^2 V^{-1} s^{-1}$ at the thickness of 110 nm. In this fashion, there is a balance between perovskite defect passivation and charge transfer. Once spin-coating the organic BHJ layer onto the perovskite surface, the strong interaction between –C=O group in PCBM and the unsaturated Pb atom can effectively passivate the defect and significantly reduce the trap state density [47]. Along with the increase of the BHJ layer thickness, the surface defects will be minimized owing to the increased interaction site. However, the further increased BHJ thickness will augment the recombination center and consequentially reduce the carrier mobility owing to the substantial interfaces between P3HT and PCBM. Therefore, the BHJ film should have high and balanced charge carrier mobility comparable to that of perovskite with the aim to make the charge transport more efficient in integrated device [23]. We further verified the proposed rule by employing other BHJ as an effective layer to enhance the performance of corresponding device, such as zinc oxide (ZnO) and polyaniline (PANi), as indicated in Fig. S5. It can be seen that the individual PANi contributes slightly to the efficiency enhancement, but a significantly enhanced PCE up to 8.44% has been obtained upon introducing ZnO into the system, suggesting that the two materials can form a BHJ at the ZnO/PANi interfaces. Therefore, the development of novel BHJ layer with high carrier mobility is crucial to further improve the efficiency of integrated perovskite/BHJ device, especially for the all-inorganic $CsPbBr_3$ PSCs.

The carrier transfer dynamics of the integrated solar cell was further investigated to understand the internal relationship between charge transport and cell efficiency. The J_{sc} and V_{oc} as a function of light intensity are plotted in Fig. 4a, b. According to $J_{sc} \propto I_L^{\alpha}$ ($\alpha \leq 1$), where I_L is the light intensity and α is an exponential factor [48], the bimolecular recombination is expected to be ideally minimal for maximal carrier output at short-circuit condition when α value is closer to 1.0 [49]. The α values are determined to be 0.95 and 0.98 for FTO/c-TiO_2/m-TiO_2/$CsPbBr_3$/carbon and FTO/c-TiO_2/m-TiO_2/$CsPbBr_3$/BHJ/carbon devices, respectively, demonstrating the bimolecular recombination is negligible and the recombination in perovskite/BHJ solar cell is not dominated by the interface recombination owing to the high carrier mobility [26,27]. Additionally, light ideality factor (n) is determined by the following equation [50]: $V_{oc} = nkT\ln(I_L)/q$ + constant. According to Shockley-Read-Hall recombination mechanism, trap-assisted re-

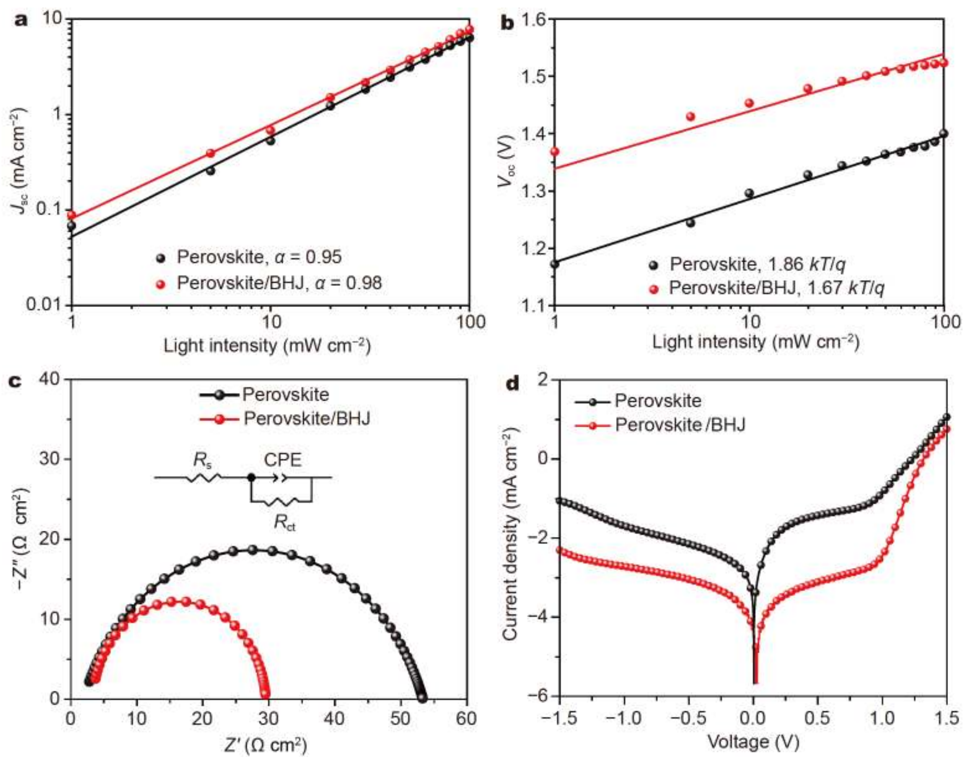

Figure 4 (a) V_{oc} and (b) J_{sc} as a function of light intensity. (c) Nyquist plots and (d) logarithmic dark current density-voltage curves of various devices with and without BHJ layer.

combination plays a dominant role when *n* approaches 2 [51]. The pristine FTO/c-TiO_2/m-TiO_2/$CsPbBr_3$/carbon PSC achieves an *n* value as high as 1.86, and it reduces to 1.67 for the BHJ-tailored device. By comparing the *α* and *n* values for various cells, the charge recombination is effectively suppressed by incorporating BHJ into the device due to reduced defects, which is mainly arisen from the passivation effect of P3HT or PCBM to the $CsPbBr_3$ film surface.

Electrochemical impedance spectroscopy (EIS) measurements were used to further explore the internal charge transfer characteristics in the dark. The EIS plots in Fig. 4c present only one semicircle, attributing to the charge transfer behavior at the interface. The series resistance (R_s) and charge transfer resistance (R_{ct}) can be extracted by fitting the Nyquist plots and the electrochemical parameters are summarized in Table S3. The R_s values (intercept of semicircle on the real axis) are almost same, while the R_{ct} values (charge-transfer resistance at the perovskite/BHJ interface) decrease obviously by incorporating BHJ into the device [52]. It suggests that the hole extraction becomes more efficient compared with pristine device owing to the inserted intermediate level between carbon and perovskite. Fig. 4d shows the logarithmic dark current density-voltage curves, and all devices exhibit a similar diode-shaped feature. The dark current of BHJ-tailored device is much lower than that of BHJ-free device in the reverse bias range. Since the current in this range is mainly dominated by shunting mechanism, the reduced dark current indicates that BHJ plays a key role in “blocking” nonradiative recombination at the perovskite/carbon interface. All the results indicate that the recombination at the perovskite/BHJ interface is significantly suppressed, promoting higher FF and J_{sc}.

Fig. 5 shows the normalized V_{oc}, J_{sc}, PCE and FF of the best BHJ-tailored $CsPbBr_3$ PSC free of encapsulation upon persistent attack by 70% relative humidity (RH) at room temperature (25°C). Obviously, the device shows a remarkable stability because the photovoltaic data are almost unchanged after storage over 75 d, which is comparable to pristine device and P3HT-tailored devices (Fig. S6). A deep observation reveals a slightly improved stability for BHJ-tailored device, which is mainly attributed to the hydrophobicity of carbon electrode and organic BHJ layer [53,54]. Till now, we can make a conclusion that the integration of BHJ with $CsPbBr_3$ can enhance charge carrier extraction, widen spectral absorption and finally increase the PCE and stability of

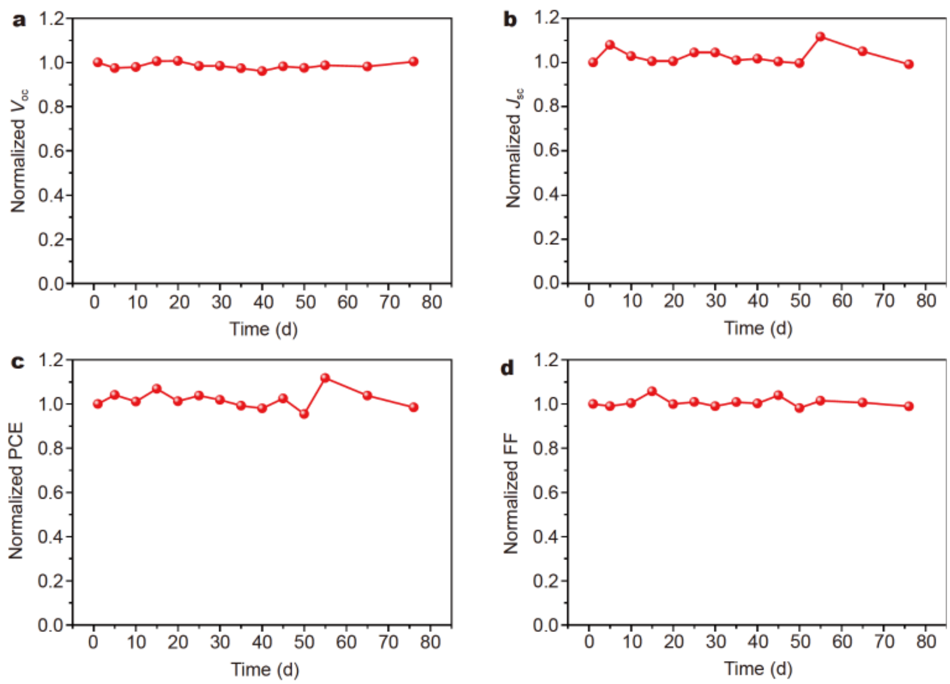

Figure 5 Normalized (a) V_{oc}, (b) J_{sc}, (c) PCE and (d) FF of $CsPbBr_3$/BHJ tailored device at 70% RH/25°C in air without encapsulation.

inorganic $CsPbBr_3$ PSC.

CONCLUSIONS

In summary, we have experimentally realized the physical proof-of-concept integrated solar cell by combining organic P3HT:PCBM BHJ with $CsPbBr_3$ to enhance the efficiency of inorganic $CsPbBr_3$ PSC. The integrated solar cell achieves an improved PCE as high as 8.94% in comparison with 6.28% for BHJ-free solar cell. The improved efficiency is mainly attributed to a wide-spectral absorption to 650 nm and efficient charge extraction. It can be predicted that higher cell efficiency would be obtained by further minimizing the charge recombination or designing more efficient narrow-bandgap donor material to maximize the light response. Under persistent attack by 70% humidity in air, the unencapsulated device presents excellent long-term stability over 75 days.

Received 29 June 2020; accepted 17 August 2020; published online 30 October 2020

1 Jung EH, Jeon NJ, Park EY, *et al.* Efficient, stable and scalable perovskite solar cells using poly(3-hexylthiophene). Nature, 2019, 567: 511–515
2 Jiang Q, Zhao Y, Zhang X, *et al.* Surface passivation of perovskite film for efficient solar cells. Nat Photonics, 2019, 13: 460–466
3 Wu T, Liu X, He X, *et al.* Efficient and stable tin-based perovskite solar cells by introducing π-conjugated Lewis base. Sci China Chem, 2020, 63: 107–115
4 Yu D, Hu Y, Shi J, *et al.* Stability improvement under high efficiency—next stage development of perovskite solar cells. Sci China Chem, 2019, 62: 684–707
5 Song W, Cao G. Surface-defect passivation through complexation with organic molecules leads to enhanced power conversion efficiency and long term stability of perovskite photovoltaics. Sci China Mater, 2020, 63: 479–480
6 Best Research-Cell Efficiency Chart, https://www.nrel.gov/pv/assets/pdfs/best-research-cell-efficiencies.20200406.pdf, accessed on 2020-04-06
7 Zhang J, Hodes G, Jin Z, *et al.* All-inorganic $CsPbX_3$ perovskite solar cells: Progress and prospects. Angew Chem Int Ed, 2019, 58: 15596–15618
8 Wang Y, Dar MI, Ono LK, *et al.* Thermodynamically stabilized β-$CsPbI_3$-based perovskite solar cells with efficiencies>18%. Science, 2019, 365: 591–595
9 Wang Y, Tu J, Li T, *et al.* Convenient preparation of $CsSnI_3$ quantum dots, excellent stability, and the highest performance of lead-free inorganic perovskite solar cells so far. J Mater Chem A, 2019, 7: 7683–7690
10 Liang J, Wang C, Wang Y, *et al.* All-inorganic perovskite solar cells. J Am Chem Soc, 2016, 138: 15829–15832
11 Chang X, Li W, Zhu L, *et al.* Carbon-based $CsPbBr_3$ perovskite solar cells: All-ambient processes and high thermal stability. ACS Appl Mater Interfaces, 2016, 8: 33649–33655
12 Duan J, Wang Y, Yang X, *et al.* Alkyl-chain-regulated charge transfer in fluorescent inorganic $CsPbBr_3$ perovskite solar cells. Angew Chem Int Ed, 2020, 59: 4391–4395
13 Huang D, Xie P, Pan Z, *et al.* One-step solution deposition of

$CsPbBr_3$ based on precursor engineering for efficient all-inorganic perovskite solar cells. J Mater Chem A, 2019, 7: 22420–22428
14 Wan X, Yu Z, Tian W, *et al.* Efficient and stable planar all-inorganic perovskite solar cells based on high-quality $CsPbBr_3$ films with controllable morphology. J Energy Chem, 2020, 46: 8–15
15 Kim M, Kim GH, Lee TK, *et al.* Methylammonium chloride induces intermediate phase stabilization for efficient perovskite solar cells. Joule, 2019, 3: 2179–2192
16 Chen T, Tong G, Xu E, *et al.* Accelerating hole extraction by inserting 2D Ti_3C_2-MXene interlayer to all inorganic perovskite solar cells with long-term stability. J Mater Chem A, 2019, 7: 20597–20603
17 Tian J, Xue Q, Yao Q, *et al.* Inorganic halide perovskite solar cells: Progress and challenges. Adv Energy Mater, 2020, 10: 2000183
18 Wang G, Dong W, Gurung A, *et al.* Improving photovoltaic performance of carbon-based $CsPbBr_3$ perovskite solar cells by interfacial engineering using P3HT interlayer. J Power Sources, 2019, 432: 48–54
19 Duan J, Zhao Y, Wang Y, *et al.* Hole-boosted $Cu(Cr,M)O_2$ nanocrystals for all-inorganic $CsPbBr_3$ perovskite solar cells. Angew Chem Int Ed, 2019, 58: 16147–16151
20 Zhang J, Bai D, Jin Z, *et al.* 3D-2D-0D interface profiling for record efficiency all-inorganic $CsPbBrI_2$ perovskite solar cells with superior stability. Adv Energy Mater, 2018, 8: 1703246
21 Jiang T, Yang YM. Efficiency breakthrough for all-perovskite tandem solar cells. Sci China Chem, 2020, 63: 294–295
22 Ye L, Fan B, Zhang S, *et al.* Perovskite-polymer hybrid solar cells with near-infrared external quantum efficiency over 40%. Sci China Mater, 2015, 58: 953–960
23 Liu Y, Chen Y. Integrated perovskite/bulk-heterojunction organic solar cells. Adv Mater, 2019, 32: 1805843
24 Guo Q, Liu H, Shi Z, *et al.* Efficient perovskite/organic integrated solar cells with extended photoresponse to 930 nm and enhanced near-infrared external quantum efficiency of over 50%. Nanoscale, 2018, 10: 3245–3253
25 Wang C, Bai Y, Guo Q, *et al.* Enhancing charge transport in an organic photoactive layer *via* vertical component engineering for efficient perovskite/organic integrated solar cells. Nanoscale, 2019, 11: 4035–4043
26 Dong S, Liu Y, Hong Z, *et al.* Unraveling the high open circuit voltage and high performance of integrated perovskite/organic bulk-heterojunction solar cells. Nano Lett, 2017, 17: 5140–5147
27 Gao K, Zhu Z, Xu B, *et al.* Highly efficient porphyrin-based OPV/perovskite hybrid solar cells with extended photoresponse and high fill factor. Adv Mater, 2017, 29: 1703980
28 Tong Y, Xiao Z, Du X, *et al.* Progress of the key materials for organic solar cells. Sci China Chem, 2020, 63: 758–765
29 Zeng G, Zhang J, Chen X, *et al.* Breaking 12% efficiency in flexible organic solar cells by using a composite electrode. Sci China Chem, 2019, 62: 851–858
30 An Q, Wang J, Gao W, *et al.* Alloy-like ternary polymer solar cells with over 17.2% efficiency. Sci Bull, 2020, 65: 538–545
31 Wu Y, Gao Y, Zhuang X, *et al.* Highly efficient near-infrared hybrid perovskite solar cells by integrating with a novel organic bulk-heterojunction. Nano Energy, 2020, 77: 105181
32 Duan J, Zhao Y, He B, *et al.* High-purity inorganic perovskite films for solar cells with 9.72 % efficiency. Angew Chem Int Ed, 2018, 57: 3787–3791
33 Liu X, Tan X, Liu Z, *et al.* Boosting the efficiency of carbon-based planar $CsPbBr_3$ perovskite solar cells by a modified multistep spin-coating technique and interface engineering. Nano Energy, 2019, 56: 184–195
34 Kim M, Kim GH, Oh KS, *et al.* High-temperature–short-time annealing process for high-performance large-area perovskite solar cells. ACS Nano, 2017, 11: 6057–6064
35 Kim J, Kim G, Back H, *et al.* High-performance integrated perovskite and organic solar cells with enhanced fill factors and near-infrared harvesting. Adv Mater, 2016, 28: 3159–3165
36 Liu Y, Hong Z, Chen Q, *et al.* Integrated perovskite/bulk-heterojunction toward efficient solar cells. Nano Lett, 2015, 15: 662–668
37 Zuo C, Ding L. Bulk heterojunctions push the photoresponse of perovskite solar cells to 970 nm. J Mater Chem A, 2015, 3: 9063–9066
38 Cheng M, Chen C, Aitola K, *et al.* Highly efficient integrated perovskite solar cells containing a small molecule-$PC_{70}BM$ bulk heterojunction layer with an extended photovoltaic response up to 900 nm. Chem Mater, 2016, 28: 8631–8639
39 Wu X, Xie L, Lin K, *et al.* Efficient and stable carbon-based perovskite solar cells enabled by the inorganic interface of CuSCN and carbon nanotubes. J Mater Chem A, 2019, 7: 12236–12243
40 Chavan RD, Tavakoli MM, Prochowicz D, *et al.* Atomic layer deposition of an effective interface layer of TiN for efficient and hysteresis-free mesoscopic perovskite solar cells. ACS Appl Mater Interfaces, 2020, 12: 8098–8106
41 Chen Y, Yang Z, Wang S, *et al.* Design of an inorganic mesoporous hole-transporting layer for highly efficient and stable inverted perovskite solar cells. Adv Mater, 2018, 30: 1805660
42 Wu C, Zou Y, Wu T, *et al.* Improved performance and stability of all-inorganic perovskite light-emitting diodes by antisolvent vapor treatment. Adv Funct Mater, 2017, 27: 1700338
43 Wang R, Xue J, Meng L, *et al.* Caffeine improves the performance and thermal stability of perovskite solar cells. Joule, 2019, 3: 1464–1477
44 Hu J, Wang C, Qiu S, *et al.* Spontaneously self-assembly of a 2D/3D heterostructure enhances the efficiency and stability in printed perovskite solar cells. Adv Energy Mater, 2020, 10: 2000173
45 Liang J, Han X, Yang J, *et al.* Defect-engineering-enabled high-efficiency all-inorganic perovskite solar cells. Adv Mater, 2019, 31: 1903448
46 Chen X, Xu W, Ding N, *et al.* Dual interfacial modification engineering with 2D MXene quantum dots and copper sulphide nanocrystals enabled high-performance perovskite solar cells. Adv Funct Mater, 2020, 30: 2003295
47 Xie J, Yan K, Zhu H, *et al.* Identifying the functional groups effect on passivating perovskite solar cells. Sci Bull, 2020, 65: 1726–1734
48 Cowan SR, Roy A, Heeger AJ. Recombination in polymer-fullerene bulk heterojunction solar cells. Phys Rev B, 2010, 82: 245207
49 Wang D, Li W, Du Z, *et al.* $CoBr_2$-doping-induced efficiency improvement of $CsPbBr_3$ planar perovskite solar cells. J Mater Chem C, 2020, 8: 1649–1655
50 Chao L, Xia Y, Li B, *et al.* Room-temperature molten salt for facile fabrication of efficient and stable perovskite solar cells in ambient air. Chem, 2019, 5: 995–1006
51 Koster LJA, Mihailetchi VD, Ramaker R, *et al.* Light intensity dependence of open-circuit voltage of polymer:fullerene solar cells. Appl Phys Lett, 2005, 86: 123509
52 Liu Y, Bag M, Renna LA, *et al.* Understanding interface engineering for high-performance fullerene/perovskite planar heterojunction solar cells. Adv Energy Mater, 2016, 6: 1501606
53 Wu M, Sun M, Zhou H, *et al.* Carbon counter electrodes in dye-

sensitized and perovskite solar cells. Adv Funct Mater, 2019, 30: 1906451

54 Wu WQ, Zhong JX, Liao JF, *et al.* Spontaneous surface/interface ligand-anchored functionalization for extremely high fill factor over 86% in perovskite solar cells. Nano Energy, 2020, 75: 104929

Acknowledgements This work was supported by the Fundamental Research Funds for the Central Universities (21620348 and 21618409), the National Natural Science Foundation of China (61774139, U1802257), and the Natural Science Foundation of Guangdong Province (2019B151502061).

Author contributions Duan J and Tang Q designed the study; Du J and Duan Y performed the experiments; Duan J and Tang Q wrote the paper. All authors contributed to the general discussion.

Conflict of interest The authors declare that they have no conflict of interest.

Supplementary information Supporting data are available in the online version of the paper.

Jian Du received his PhD degree in the fields of electrochemistry from Qingdao Institute of Bioenergy and Bioprocess Technology, Chinese Academy of Sciences in 2019. Currently, he is a Postdoctoral Researcher in the College of Information Science and Technology at Jinan University (Guangzhou, China). His research interests focus on perovskite materials, inorganic nanomaterials and their applications in photovoltaic devices and triboelectric nanogenerators for sustainable and clean energy.

Jialong Duan received his PhD degree from Ocean University of China in 2019. After graduation, he became an Associate Professor in the College of Information Science and Technology at Jinan University (Guangzhou, China). His research interests focus on the all-inorganic perovskite solar cells, dye-sensitized solar cells and nanogenerators.

Qunwei Tang is a full Professor in the College of Information Science and Technology at Jinan University (Guangzhou, China). After receiving his PhD at Huaqiao University in 2009, he joined Strasbourg University and the University of South Carolina as a postdoctoral fellow. He joined Ocean University of China in 2012 and moved to Jinan University in 2018. His research interests cover inorganic perovskite solar cells and triboelectric nanogenerators.

利用有机体相异质结增强$CsPbBr_3$钙钛矿太阳能电池的电荷提取以及光谱吸收

杜健[1], 段加龙[1*], 段艳艳[2], 唐群委[1*]

摘要 全无机$CsPbBr_3$钙钛矿太阳能电池能够很好地平衡传统杂化器件的效率和稳定性问题. 然而，较大的电荷传输势垒以及较窄的吸光范围已经成为限制器件效率进一步提升的两大挑战. 本文通过构建有机体相异质结(P3HT:PCBM光活性层)加速器件电荷提取并扩宽吸光范围, 通过进一步优化P3HT:PCBM光活性层的厚度, 获得了8.94%的光电转换效率, 远高于单一$CsPbBr_3$作为吸光层的电池效率(6.28%). 通过系统的测试表征发现PCBM中的羰基与钙钛矿表面未饱和的铅原子相互作用能够有效地钝化缺陷态，减小器件的复合反应. 另外，PCBM和P3HT之间的相互耦合将器件的吸光范围扩宽至650 nm，能够在不降低电池开路电压的前提下增加光生载流子的数量，提高电池器件的短路电流. 尤为重要的是，器件在70%相对湿度下存放75天仍能保持相对稳定. 高效、稳定、可大规模制备的优势能够加速无机钙钛矿太阳能电池的商业化进程.

